Experimental study of critical behavior of three-dimensional Heisenberg ferromagnets with small anisotropy: $CuM_2X_4 \cdot 2H_2O$ (M = NH₄ or K, X = Br or Cl)†

E. Velu, J.-P. Renard, and B. Lecuyer

Institut d'Electronique Fondamentale, Laboratoire associé au Centre National de la Recherche Scientifique, Bâtiment 220,
Université Paris XI, 91405 Orsay Cedex, France

(Received 24 November 1975)

We have measured the parallel and perpendicular susceptibilities, the spontaneous magnetization and the induced magnetization of $Cu(NH_4)_2Br_4 \cdot 2H_2O$, $CuRb_2Br_4 \cdot 2H_2O$, and $CuK_2Cl_4 \cdot 2H_2O$. These measurements have permitted us to determine the intensity of the exchange anisotropy and the critical exponents β, γ, and δ as well as the form of the state equation of bromine compounds. Near the Curie temperature, the experimental state equation is close to the theoretical one of the three-dimensional Heisenberg model and the scaling laws are approximately fulfilled. The measured susceptibilities agree with the theoretical results for the slightly anisotropic Heisenberg ferromagnet. The crossover due to the small uniaxial anisotropy is clearly observed on the perpendicular susceptibility and permits the explanation of the low experimental value of γ.

I. INTRODUCTION

In order to study the critical behavior of the three isomorphous salts $Cu(NH_4)_2Br_4 \circ 2H_2O$, $CuRb_2Br_4 \cdot 2H_2O$, and $CuK_2Cl_4 \circ 2H_2O$, we have measured their susceptibilities, their spontaneous magnetization, and induced magnetization in a magnetic field. These salts are insulators presenting a paraferromagnetic transition at the respective Curie temperatures of 1.83, 1.87, and 0.89 K. Their structure is particularly simple because the copper lattice is tetragonal and almost bcc (Sec. II). Their magnetic and thermodynamic properties are well interpreted by the $S = \frac{1}{2}$ Heisenberg model with interactions between nearest and next-nearest neighbors[1,2] and small uniaxial exchange anisotropy. Using the perpendicular magnetic susceptibility $\chi_\perp$ (Sec. IV C) and the low-temperature properties of the spontaneous magnetization[3] (Sec. V B), we evaluate the relative intensity of the anisotropy at 6×10^{-3} for the bromine compounds and at 3×10^{-3} for $CuK_2Cl_4 \cdot 2H_2O$.

The simplest mechanism to explain the presence of the anisotropy is that of the pseudodipolar exchange. The fundamental state of a copper ion Cu^{2+} placed in an orthorhombic symmetric crystal field is a Kramer's doublet. Owing to the spin-orbit coupling, the two components of the doublet are mixtures of spin-up and spin-down states. At low temperature, if the exchange interaction between spins is much weaker than the energy of the first excited level, then all ions are in their fundamental state, and we can consider that each one of them is a system with two levels, that is to say equivalent to a pure fictitious $\sigma = \frac{1}{2}$ spin with a Landé factor g slightly different from 2. The Heisenberg exchange interaction $-\sum_{ij} J_{ij} \vec{S}_i \cdot \vec{S}_j$ is treated as a perturbation. It expresses itself in terms of fictitious spins σ by

$$-\sum_{ij} (J_{ijx}\sigma_{ix}\sigma_{jx} + J_{ijy}\sigma_{iy}\sigma_{jy} + J_{ijz}\sigma_{iz}\sigma_{jz}).$$

Therefore, if we consider the copper ions as pure fictitious $\sigma = \frac{1}{2}$ spins, the exchange is necessarily anisotropic. The relative intensity of the anisotropy is of the order of $(\Delta g/g)^2$, where $\Delta g/g$ is the relative anisotropy of the Landé factor. For the salts studied here, we have $(\Delta g/g)^2 \sim 10^{-2}$. Thus, the pseudodipolar exchange mechanism qualitatively explains the observed anisotropy.

Owing to their small axial anisotropy, the studied ferromagnets are highly suitable to check the effect of anisotropy on critical behavior. Riedel and Wegner[4] were the first to predict a crossover due to the exchange anisotropy from Heisenberg critical behavior to Ising critical behavior. Their theory predicts in our case that the reduced temperature of cross over is about 10^{-2}, which is in our experimental range. This crossover is easy to observe by comparing the parallel $\chi_{\parallel}$ and perpendicular $\chi_\perp$ susceptibilities in the critical zone. Moreover, the recent works of Pfeuty *et al.*[5] permit us to compare our experimental results with precise, numerical calculations (Sec. VII C).

In these salts there also exist dipolar interactions between spins that may produce a crossover from the Heisenberg model to the isotropic dipolar model.[6] These dipolar interactions have already been used to explain the experimental value of the critical exponent α relative to the specific heat.[7] Their influence is discussed in Sec. VII C.

This paper is organized as follows: in Sec. II we give a brief account of the crystal structure of the salts studied. In Sec. III we give some experimental details on the measurement and control of the temperature. Section IV describes the measurements of the magnetic susceptibilities. The low-temperature measurements of $\chi_\perp$ permit us

to evaluate the anisotropy. In Sec. V. we describe some experiments using nuclear magnetic res-onance (NMR). They allow us to obtain the re-duced spontaneous magnetization curve $m_s(T)$. For $T < T_c$, the curve $m_s(T)$ gives us a second evaluation of the anisotropy. The anisotropy of $CuK_2Cl_4 \cdot 2H_2O$ is discussed in detail.

In Sec. VI, we give the results of the measure-ments of magnetization induced by a magnetic field H. Finally, in Sec. VII, all our results rela-tive to the neighborhood of T_c are discussed: the critical exponents, the scaling laws, the state equation, and the crossovers due to the anisotropy and to the dipolar interactions.

II. CRYSTALLOGRAPHIC STRUCTURE

The $CuK_2Cl_4 \cdot 2H_2O$ crystals are obtained by the slow evaporation at room temperature of a satu-rated aqueous solution containing 1 mole of $CuCl_2$ for each mole of KCl. The bromine compounds are obtained by the same process except that the components are in stoichiometric proportions. As the presence of chlorine impurities in the bro-mine compounds modifies their critical tempera-ture (Fig. 8), we have used the purest possible components: $CuBr_2$ is produced from CuO (Cl $< 10^{-3}$ wt.%) and HBr (Cl $< 10^{-2}$ wt.%) RbBr con-tains less than 10^{-5} wt.% of Cl and NH_4Br less than 0.2 wt.%, so that, for each atom of Br, we find in the solutions less than 10^{-4} atoms of Cl for $CuRb_2Br_4 \cdot 2H_2O$ and less than 3×10^{-3} atoms of Cl for $Cu(NH_4)_2Br_4 \cdot 2H_2O$.

$CuK_2Cl_4 \cdot 2H_2O$ and $Cu(NH_4)_2Br_4 \cdot 2H_2O$ belong to the space group $P4_2/mnm$.[8] The unit cell is a rectangular parallelepiped with a square base of side a and height c (Fig. 1, Table I). The copper ions are located at the corner and in the center of this unit cell. The ratio c/a is 1.05, so that the copper lattice is almost body-centered cubic. In all the theoretical calculations, we have made the simplifying hypothesis of a bcc lattice.

Each copper atom is surrounded by four halogens forming a rhombus whose plane is perpendicular to the [001] axis and whose diagonals are parallel to [110] and [1$\bar{1}$0]. The furthest halogen from the copper is noted $X(I)$, the closest $X(II)$. The local copper axes parallel to the directions Cu-$X(I)$ and Cu-$X(II)$ are called [γ] and [γ'], respectively. The local axes of the copper situated in the center of the unit cell make a 90° angle with those of the copper located at the corner of the unit cell.

There are no crystallographic data for $CuRb_2Br_4 \cdot 2H_2O$; but as the natural crystals of the salt are identical to those of $Cu(NH_4)_2Br_4 \cdot 2H_2O$ and the NMR spectra of the two salts are very similar, we can conclude that they have the same structure.
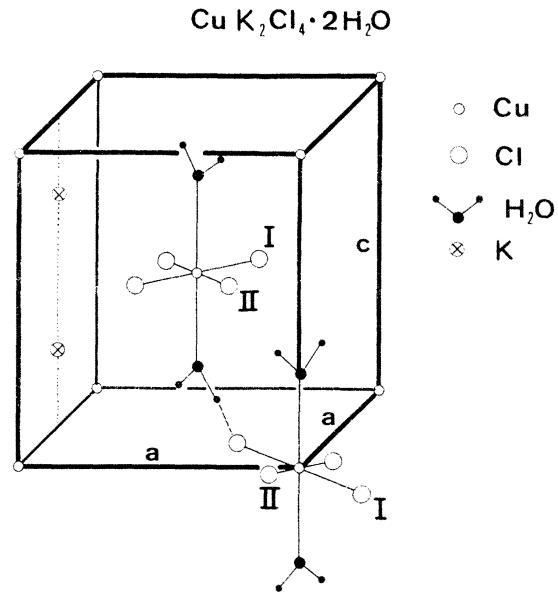

FIG. 1. Crystal structure of $K_2CuCl_4 \cdot 2H_2O$.

The densities of $CuK_2Cl_4 \cdot 2H_2O$ and $Cu(NH_4)Br_4 \cdot 2H_2O$ are calculated from the crystal parameters. That of $CuRb_2Br_4 \cdot 2H_2O$ was determined by mea-suring the Archemedian pressure produced by a bath of dibutyl phthalate on a crystal of known mass.

III. CONTROL AND MEASUREMENT OF THE TEMPERATURE

The temperatures between 1.2 and 4.2 K are ob-tained in a bath of pumped ^{4}He and those between 0.35 and 1.2 K in a bath of pumped ^{3}He.

Below 2.17 K, the ^{4}He is superfluid and is a good conductor of heat. An automatic control of the temperature is therefore obtained with a 47 Ω, $\frac{1}{8}$ W Allen Bradley resistance and a heating resis-tance of 100 Ω. The heating powers are usually 20 mW. The stability of the temperature is better than 2×10^{-4} K in the neighborhood of 1.8 K.

The temperature is measured by another 47 Ω, $\frac{1}{8}$ W Allen Bradley resistance placed near the sample. The resistance R is related to the tem-perature by the empirical law of Clement and Quinnell[9]

TABLE I. Unit-cell dimensions and density.

	a (Å)	c (Å)	Density (g/cm^3)
$CuK_2Cl_4 \cdot 2H_2O$	7.477	7.935	2.40
$Cu(NH_4)_2Br_4 \cdot 2H_2O$	7.98	8.41	2.82
$CuRb_2Br_4 \cdot 2H_2O$	$\cdots$	$\cdots$	3.71 ± 0.04

$$\log_{10}R + \lambda/\log_{10}R = A + B/T. \tag{1}$$

In each run, the resistance is calibrated from about ten data points, where the temperature is computed according to the pressure of the helium above the cryogenic bath (1958 scale). The coefficients λ, A, and B are determined by the method of least squares. The difference between the temperature computed according to the resistance and the temperature computed according to the pressure remains smaller than 1 mK in the interval 1.5–2.17 K.

Between 2.17 and 4.2 K, the automatic control does not function well because of the great time constant of heat transfers. The vapor pressure of ^{4}He is regulated by a Cartesian manostat which acts upon the flow of the pumping. The temperature stability thus obtained is sufficient for the experiments undertaken. The temperature is measured by a 47 Ω, $\frac{1}{8}$ W Allen Bradley resistance calibrated from a measure at 4.2 K and from a few measures between 1.5 and 2.17 K. Using the susceptibility of a chromium potassium alum (Fig. 2), we checked once that our interpolation process using the law of Clement and Quinnell between 2.17 and 4.2 K gives the correct temperature.

Between 0.35 and 1.2 K, the speed of pumping of the ^{3}He is regulated manually with the help of a needle valve. The stability of the temperature is better than 0.3 mK in the neighborhood of 0.9 K. The temperature is measured by a 10 Ω, $\frac{1}{8}$ W Allen Bradley resistance calibrated between 0.7 and 1.2 K from the vapor pressure of ^{3}He (1962 scale). Below 0.7 K, the thermomolecular correction becomes non-negligible. We obtain a first estimate of the temperature T_R by extrapolating the law of Clement and Quinnell [Eq. (1)] obtained between 0.7 and

1.2 K. This temperature T_R was compared to the temperature T deduced from the susceptibility of a cerium magnesium double nitrate crystal. We deduce from this experiment the following empirical law, which holds between 0.32 and 0.7 K:

$$T = T_R - 10^{-3}T_R^{-2.5}. \tag{2}$$

IV. MAGNETIC SUSCEPTIBILITIES

The measurement apparatus is an ac mutual inductance bridge functioning at frequencies of about 70 Hz.[10] The measurement coil, immersed in ^{4}He, is made up of two theoretically opposite mutuals. In fact, in the absence of a sample, the mutual of the coil is not zero: we denote it μ_0. When the sample is placed in one of the mutuals, the total mutual of the coil becomes

$$\mu_t = \mu_0 + kV\chi_a, \tag{3}$$

where V is the volume of the sample, χ_a is the apparent volumic susceptibility of the sample, k is the calibration factor, and μ_t is measured in the bridge by a calibrated mutual.

In ^{4}He, the sample can be taken out of the coil in the course of the experiment in such a way that μ_0 can be accurately determined at that moment. In ^{3}He, we cannot take out the sample and μ_0 is determined from an experiment without sample.

The calibration factor k is calculated from the susceptibilities of spheres of chromium alum, of ammonium magnesium sulfate, and of ferrite (Fig. 2). The measurement of μ_t therefore gives the apparent volumic susceptibility χ_a. The true volumic susceptibility χ can then be computed, using the relation

$$1/\chi_a = 1/\chi + N. \tag{4}$$

N is the demagnetizing factor. In order to have a homogeneous and relatively small demagnetizing factor, we cut our samples into ellipsoids prolate in the direction of the measurement of susceptibility.

At $T < T_c$, in the bromine compounds, the apparent susceptibility measured along the [001] direction reaches the theoretical limit imposed by the demagnetizing factor, if one takes into account experimental error. On the other hand, perpendicularly to [001], it remains smaller than this limit. We can thus conclude that there exists only one easy axis, [001].

In $CuK_2Cl_4 \cdot 2H_2O$, the apparent volumic susceptibility is isotropic in the plane perpendicular to [001]. Below $T_c = 0.89$ K, it reaches the inverse of the demagnetizing factor, when one takes into account the experimental error. On the contrary, along the [001] direction, it does not reach this limit. We conclude that the easy axes are perpen-
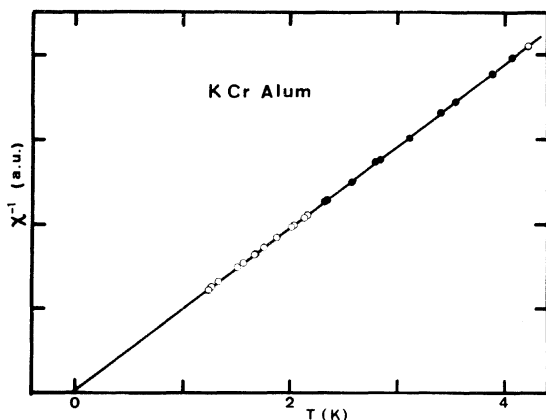

FIG. 2. Calibration of the susceptibility measurements bridge. $\bigcirc$: the temperature is calculated from the vapor pressure of ^{4}He; $\bullet$: the temperature is calculated by interpolation of the Clement and Quinnell law.

TABLE II. Experimental and theoretical critical parameters for the $S = \frac{1}{2}$ bcc Heisenberg model.

	$CuK_2Cl_4 \cdot 2H_2O$	Nearest-neighbor interaction	Next-nearest neighbor interaction	Third-neighbor interaction
T_c/θ	0.72	0.63	0.70	0.81
$\dfrac{S_\infty - S_c}{R}$	0.222 [a]	0.235	0.210	$\cdots$
$-\dfrac{E_c}{RT_c}$	0.384 [a]	0.460	0.357	$\cdots$

[a] See Ref. 11.

dicular to [001].

We call parallel susceptibility $\gamma_\parallel$ the susceptibility along an easy axis and perpendicular susceptibility, $\chi_\perp$, the susceptibility along a direction perpendicular to all easy axes.

A. $T > 2T_c$

The study of the susceptibilities at $T > 2T_c$ enables us to determine the range of the exchange interaction. Analyzing the specific-heat measurements of Miedema et al.[11] for $Cu(NH_4)_2Br_4 \cdot 2H_2O$ and $CuK_2Cl_4 \cdot 2H_2O$, Wood and Dalton[1] concluded that in these salts, the exchange interaction between next-nearest neighbors, J_2, is about $\frac{1}{4}$ of the interaction between nearest neighbors, J_1. Van Amstel and de Jongh[2] have recently shown that, in $Cu(NH_4)_2Br_4 \cdot 2H_2O$ and $CuRb_2Br_4 \cdot 2H_2O$, J_2 is almost equal to J_1 and that perhaps there exists an interaction between third neighbors J_3.

We have studied $CuK_2Cl_4 \cdot 2H_2O$ in a similar manner.[12] Its relatively low critical temperature permits us to reach temperatures of $4.7T_c$, and to measure the Curie-Weiss temperature θ. For $2T_c < T < 4.7T_c$, the ratio $\chi T/C$ (C is the Curie constant) is perfectly isotropic; this shows that the influence of the possible anisotropy is negligible at this temperature. The measured Curie-Weiss temperature is 1.24 K. The ratio T_c/θ is equal to 0.72. This ratio theoretically depends on the number of equivalent neighbors.[13,14] Here we find 16 equivalent neighbors: thus the next-nearest-neighbor interaction is nearly equal to the nearest-neighbor interaction. The experimental values of other critical parameters support this hypothsis (Table II).

Lastly, we compared the susceptibility of $CuK_2Cl_4 \cdot 2H_2O$ to the high-temperature series expansion of the Heisenberg Hamiltonain[13,15] (Fig. 3). The theoretical curve computed for $J_2 = J_3 = 0$ is valid for $T/T_c > 1.5$. The curves computed for J_2 and $J_3 \neq 0$ are valid only for $T/T_c > 2$ because of the small number of known terms in the expan-

sion. The fit is very good with the theoretical curve computed for $J_1 = J_2$ and $J_3 = 0$.

B. Parallel susceptibility in the neighborhood of T_c

In the neighborhood of T_c, we have tried to fit the thermal dependence of the parallel susceptibility with the law

$$\chi_\parallel = \Gamma \epsilon^{-\gamma}, \tag{5}$$

where $\epsilon = (T - T_c)/T_c$.

In order to avoid the errors due to the uncertainty of the T_c value, we use the Kouvel and Fisher method[16] to analyze the data. Thus we plot $-\chi_\parallel (d\chi_\parallel/dT)^{-1}$ vs T. If Eq. (5) is true, this curve is a straight line which intersects the T axis at T_c (Fig. 4). This is observed for the three salts. We compute the T_c value by the least-squares method, and we plot the curve $\log_{10}\chi_\parallel$ vs $\log_{10}\epsilon$ (Fig. 14). The coefficients Γ and γ are determined by the least-squares method. The experimental values of T_c, γ, $\Gamma T_c/C$, and the validity interval of Eq. (5) are given in Table III.
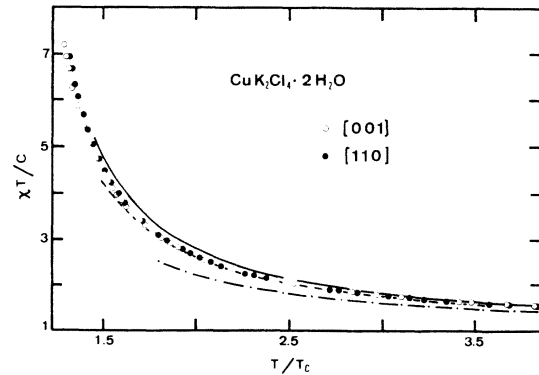

FIG. 3. Experimental susceptibilities of $CuK_2Cl_4 \cdot 2H_2O$ compared with the high-temperature series expansions computed for the $S = \frac{1}{2}$ bcc Heisenberg model: (——): $J_2 = J_3 = 0$ (Ref. 15); (----): $J_1 = J_2 \neq 0$, $J_3 = 0$ (Ref. 13); (—·—): $J_1 = J_2 = J_3$ (Ref. 13).
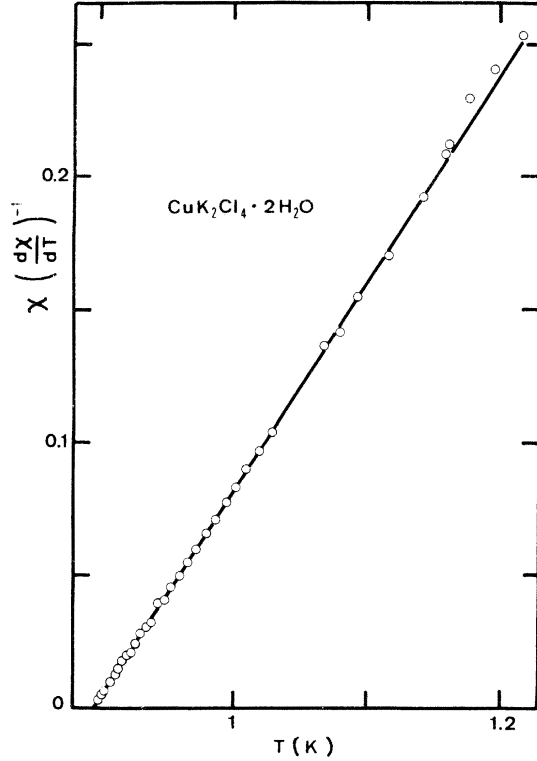
FIG. 4. Determination of T_c by the Kouvel and Fisher method for $CuK_2Cl_4 \cdot 2H_2O$.

C. Perpendicular susceptibility for $T < 0.5\ T_c$: evaluation of the anisotropy

The field dependence and the temperature dependence of the perpendicular susceptibility at low temperature allow us to evaluate the intensity of the anisotropy.

1. Field dependence of perpendicular susceptibility

We have studied the influence of the anisotropy on the field dependence of $\chi_\perp$ using the molecular field approximation (Appendix A). The theoretical results, which are known to hold at 0 K, are shown in Figs. 15(a) and 15(b). The behavior of $\chi_\perp$ in the presence of a magnetic field parallel to an easy axis or to the measurement axis of $\chi_\perp$, theoretically enables us to determine H_A, the anisotropy field defined by Eq. (A2).

This has led us to measure $\chi_{\perp a}$ in the presence of a field parallel to the measurement axis of $\chi_{\perp a}$ in the case of $CuRb_2Br_4 \cdot 2H_2O$ and $CuK_2Cl_4 \cdot 2H_2O$, and of a field parallel to the easy axis [001] in the case of $CuRb_2Br_4 \cdot 2H_2O$. The experimental curves plotting $\chi_{\perp a}$ versus the field are shown in Figs. 5(a) and 5(b). The curves obtained for the lowest temperature $T \sim 0.35$ K are the only ones which are approximately of the shape predicted by molecular field theory; they enable us to estimate H_A. Table IV contains the results.

2. Temperature dependence of the perpendicular initial susceptibility

The temperature dependence of $\chi_\perp$ is qualitatively the same for the three salts. When T decreases, $\chi_\perp$ reaches a maximum at $T = T_c$, then decreases more and more slowly until T reaches 0 K. The $\chi_\perp$ value at 0 K gives us an estimate of H_A [Eq. (A6) and Appendix B].

$$\frac{\chi_\perp (0\ \text{K})}{ng_\perp \mu_B S} = \frac{g_\perp}{g_\parallel} \frac{1}{H_A}. \tag{6}$$

In $CuRb_2Br_4 \cdot 2H_2O$, we compare the temperature dependence of $\chi_\perp$ with the theoretical curve [Eq. (B16)] (Fig. 6). The value of $\chi_\perp$ (0 K) = 30.3 emu

TABLE III. Experimental values of T_c, γ, and $\Gamma T_c/C$ deduced from the susceptibility measurements.

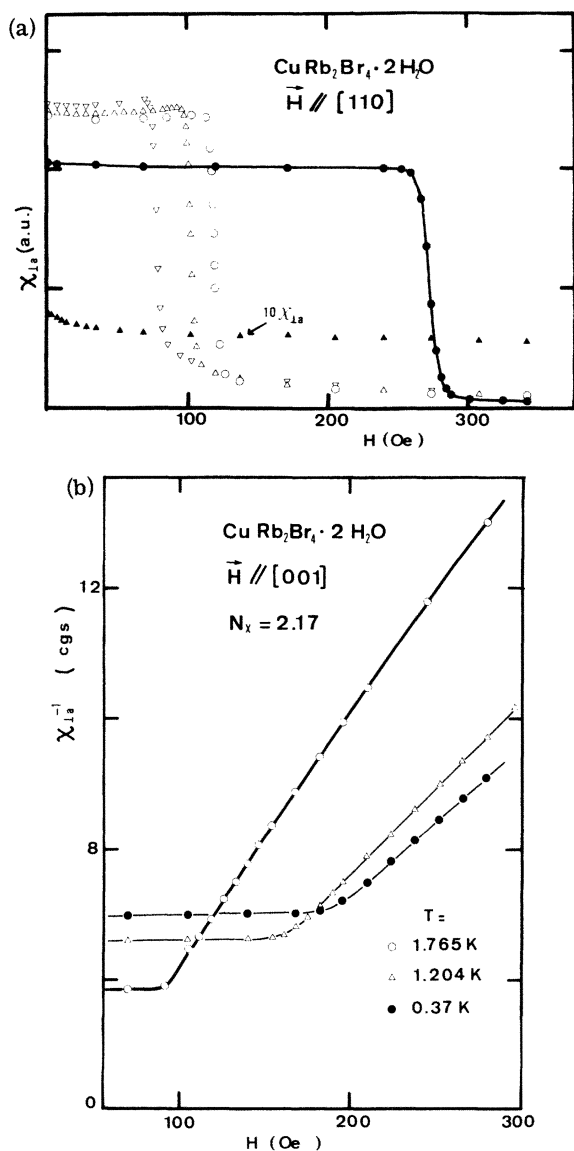|	$Cu(NH_4)_2Br_4 \cdot 2H_2O$	$CuRb_2Br_4 \cdot 2H_2O$	$CuK_2Cl_4 \cdot 2H_2O$
Kouvel and Fisher method	$2 \times 10^{-3} < \epsilon < 10^{-1}$	$8.5 \times 10^{-3} < \epsilon < 7 \times 10^{-2}$	$5 \times 10^{-3} < \epsilon < 1.5 \times 10^{-1}$
T_c	1.827 ± 0.002 K	1.8739 ± 0.0005 K	0.8957 ± 0.0003 K
γ	1.26 ± 0.02	1.28 ± 0.015	1.28 ± 0.01
$\log \chi_\parallel$ vs $\log \epsilon$	$2 \times 10^{-3} < \epsilon < 2.2 \times 10^{-1}$	$5 \times 10^{-3} < \epsilon < 3 \times 10^{-1}$	$1.5 \times 10^{-3} < \epsilon < 3 \times 10^{-1}$
γ	1.275 ± 0.017	1.29 ± 0.01	1.28 ± 0.01
$\Gamma T_c/C$	1.22 ± 0.08	1.26 ± 0.05	1.27 ± 0.05
Suzuki and Watanabe (Ref. 17)	$2 \times 10^{-3} < \epsilon < 10^{-1}$	$\cdots$	$\cdots$
T_c	1.831 ± 0.001 K	$\cdots$	$\cdots$
γ	1.30 ± 0.03	$\cdots$	$\cdots$
De Jongh and Miedema (Ref. 18)	$8 \times 10^{-3} < \epsilon < 3 \times 10^{-1}$	$\cdots$	$\cdots$
T_c	1.773 ± 0.001 K	$\cdots$	$\cdots$
γ	1.31 ± 0.02	$\cdots$	$\cdots$
$\Gamma T_c/C$	1.22 ± 0.15	$\cdots$	$\cdots$

(a)

FIG. 5. Experimental variation of the apparent perpendicular susceptibility of $CuRb_2Br_4 \cdot 2H_2O$, as a function of the applied field. (a) Field is parallel to the direction along which $\chi_\perp$ is measured. ●: $T = 0.35$ K; ○: T = 1.829 K; △: $T = 1.75$ K; ▽: $T = 4.2$ K; ▲: $T = 1.785$ K. Ordinate of the experimental data at $T = 4.2$ K is multiplied by ten. (b) Field is parallel to the easy axis [001].

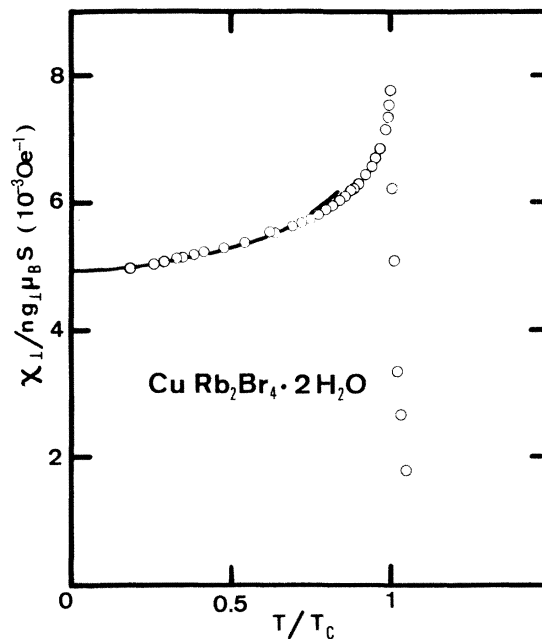FIG. 6. Temperature dependence of the true perpendicular susceptibility of $CuRb_2Br_4 \cdot 2H_2O$ for $T < T_c$. (——): theoretical curve computed with the help of Eq. (B16) for $H_A = 220$ Oe.

cgs/mole is chosen in order to have a good fit between the experiments and the theory. This fit is very satisfactory below $T/T_c = 0.7$. The anisotropy field deduced from $\chi_\perp$ (0 K) is 220 ± 13 Oe. The uncertainty arises especially from the uncertainties in the demagnetizing factor and in the calibration factor of the bridge used in the susceptibility measurements.

For $Cu(NH_4)_2Br_4 \cdot 2H_2O$, we did no experiments at very low temperature, but, in the observed domain $0.65 < T/T_c < 1$, $\chi_\perp$ is very close to the value of $\chi_\perp$ for $CuRb_2Br_4 \cdot 2H_2O$. We conclude that $\chi_\perp$ (0 K) = 29 emu cgs/mole, and therefore that H_A = 230 ± 15 Oe.

For $CuK_2Cl_4 \cdot 2H_2O$ the minimal attainable temperature is still too high to allow us to accurately compare $\chi_\perp$ with the theoretical curve. In that case, the apparent susceptibility is three times that of the bromine compounds and closer to the

TABLE IV. Anisotropy field values deduced from the perpendicular susceptibility measurements (in Oe).

	$\chi_\perp$ (0 K)	$\chi_\perp$ in presence of a field perpendicular to the easy axes	$\chi_\perp$ in presence of a field parallel to an easy axis
$CuRb_2Br_4 \cdot 2H_2O$	220 ± 13 at 0 K	203 ± 20 at 0.35 K	206 ± 20 at 0.37 K
$Cu(NH_4)_2Br_4 \cdot 2H_2O$	230 ± 15 at 0 K	$\cdots$	$\cdots$
$CuK_2Cl_4 \cdot 2H_2O$	52 ± 6 at 0 K	44 ± 5 at 0.36 K	$\cdots$

TABLE V. Mean NMR frequency of the protons at $T = 0$ K and anisotropy field deduced from the low-temperature spontaneous magnetization.

	$Cu(NH_4)_2Br_4 \cdot 2H_2O$	$CuRb_2Br_4 \cdot 2H_2O$	$CuK_2Cl_4 \cdot 2H_2O$
$\nu(0)$ (MHz)	6.450 ± 0.005	6.473 ± 0.001	3.664 ± 0.002
H_A (Oe)	$245 \quad \pm 25$	$250 \quad \pm 25$	$\cdots$

demagnetizing factor. The uncertainty for the true susceptibility reaches 12%. However, we can roughly extrapolate the curve at 0 K and obtain the value $\chi_\perp$ (0 K) = 102 ± 12 emu cgs/mole, which is equivalent to an anisotropy field of 52 ± 6 Oe. The results of the different measurements of H_A are given in Table V. All these values are consistent when we take into account that the anisotropy field measured at 0.36 K is less than the one at 0 K. The H_A value found for the bromine compounds agrees with that of 200 Oe deduced by Suzuki and Watanabe[19] from EPR in $Cu(NH_4)_2Br_4$ $\cdot 2H_2O$. Lastly, the experiments of susceptibility are properly explained if we assume that the Hamiltonian of the three salts is given by

$$\mathcal{3C}_0 = - \sum_{ij} J_{ij}\vec{S}_i \cdot \vec{S}_j - \sum_{ij} K_{ij}S_{iz}S_{jz},\qquad (7)$$

where z is the [001] axis and the sums $\sum_{ij}$ are extended to the nearest and next-nearest neighbors i and j.

In the bromine compounds, the anisotropy is uniaxial: $\sum_{ij}K_{ij} > 0$ and its relative intensity is

$$\sum_{ij} K_{ij} \Big/ \sum_{ij} J_{ij} \simeq 6 \times 10^{-3}.$$

In $CuK_2Cl_4 \cdot 2H_2O$, the anisotropy is planar: $\sum_{ij}K_{ij} < 0$ and its relative intensity is

$$\left| \sum_{ij} K_{ij} \right| \Big/ \sum_{ij} J_{ij} \simeq 3 \times 10^{-3}.$$

V. SPONTANEOUS MAGNETIZATION

The spontaneous magnetization of the three salts is obtained by NMR of the halogens and of the protons of water. The nuclear resonance frequencies depend on the local magnetic field at the site of the nucleus. When no field is applied, the local-field intensity is usually rigorously proportional to the magnetization of the magnetic ions and its direction strongly depends on the direction of the magnetization. We can therefore accurately study the spontaneous magnetization by NMR, even in the neighborhood of the critical point.

A very complete study of the NMR in the salts isomorphous to $CuK_2Cl_4 \cdot 2H_2O$ was done simultaneously and independently of us by Klaassen et al.[20] We therefore only report our results relative to the anisotropy and to critical behavior.

A. NMR of halogens: spontaneous magnetization near T_c

The ^{81}Br and ^{35}Cl nuclei have a nuclear spin-$\frac{3}{2}$ and a quadrupole moment which interacts with the local electric field gradient (EFG) at the site of the nucleus. If the local magnetic field is zero, we observe one pure quadrupole resonance line of frequency ν_Q. If the local field H_l is nonzero, we note $\nu_H = (\gamma/2\pi)H_l$, where γ is the nuclear gyromagnetic ratio. In the case where $\nu_H \ll \nu_Q$ and H_l is parallel to one of the EFG axes, the pure quadrupole line is split into four lines, the intensities of which vary according to the orientation of the radio frequency field exciting the resonance. The spectrum is symmetric with respect to ν_Q, up to first order in ν_H/ν_Q. The difference between the frequencies of two of the lines is rigorously equal to $2\nu_H$, and therefore proportional to H_l. All experiments are done without an external magnetic field in such a way that H_l is proportional to the spontaneous magnetization, in the ferromagnetic state, and zero in the paramagnetic state. The local field at the halogen site is parallel to one of the EFG axes because of the crystal symmetry.

The behavior of the two bromine compounds is quite similar. We observe two distinct ^{81}Br spectra corresponding to the two sites Br(I) and Br(II) and to one easy axis [001]. When the temperature decreases from 4.2 K to T_c, we notice that the pure quadrupole line of $^{81}Br(I)$ remains at the same frequency ν_Q but becomes broader. It nevertheless remains detectable. Below T_c, it splits into four lines whose frequencies are close to ν_Q and whose splittings increase when the temperature decreases. The splitting between the two exterior lines is proportional to the spontaneous magnetization [Fig. 7(a)].

The temperature where the ferromagnetic lines appear theoretically coincides with the Curie temperature. In fact, over a temperature range of about 1 mK, we observe a coexistence of the ferromagnetic lines and the paramagnetic pure quadrupole line.[21] Near T_c, the lines are clearly asymmetrical. We conclude from this that the critical temperature is not homogeneous in the sample. This effect is particularly perceptible for $Cu(NH_4)_2Br_4 \cdot 2H_2O$ and we believe that it is due to the presence of chlorine impurities. In fact, we have noted that the $Cu(NH_4)_2Br_4 \cdot 2H_2O$ crystals

grown from solutions containing chlorine impurities have a Curie temperature noticeably lower than that of a purer crystal (Fig. 8): $\Delta T_c \simeq -14$ mK for 1% chlorine impurities in the solution. Finally, the chosen Curie temperature is the
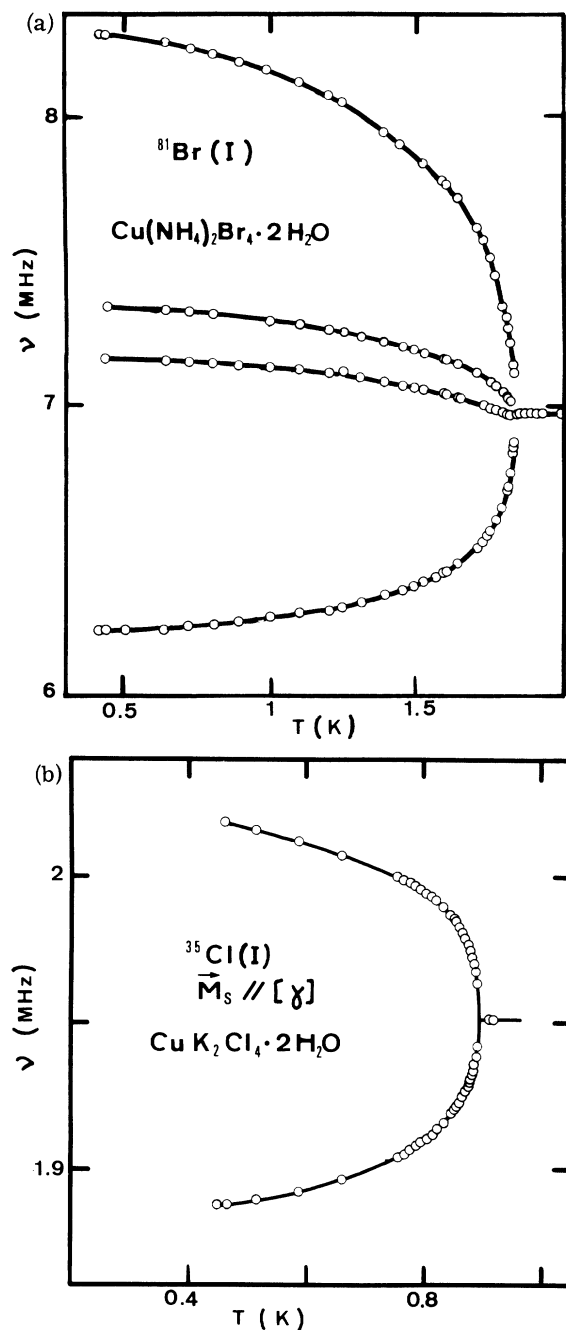
minimal temperature where only the pure quadrupole line is visible. It may vary slightly from one sample to another because of impurities (Table VI).

For $CuK_2Cl_4 \cdot 2H_2O$, the existence of four distinct ^{35}Cl spectra clearly shows that there are two easy axes, [110] and [1$\bar{1}$0].[20] The $^{35}Cl(I)$ spectrum for spontaneous magnetization parallel to [γ] [Fig. 7(b)] is the only one to permit us to determine M_s near T_c. The distance between the two detectable lines is proportional to M_s.

For the three salts, the reduced spontaneous magnetization near T_c is well fitted by the law (Fig. 9)

$$m_s = B|\epsilon|^\beta. \tag{8}$$

The amplitude B and the exponent β are computed by the least squares method. All results are given in Table VI. Two $Cu(NH_4)_2Br_4 \cdot 2H_2O$ samples of different purities were used, but we have observed no difference for the critical parameters β and B.

B. NMR of protons: low-temperature spontaneous magnetization

In the ferromagnetic state, when no field is applied, the NMR spectrum of the protons of a water molecule is composed of four to six lines, sym-

FIG. 7. NMR spectrum of the halogen (I). (a) $^{81}Br(I)$ in $Cu(NH_4)_2Br_4 \cdot 2H_2O$. (b) $^{35}Cl(I)$ in $CuK_2Cl_4 \cdot 2H_2O$ in the case where the spontaneous magnetization is parallel to the direction Cu-Cl(I). Two other lines with a larger splitting exist but they are too weak to be detected.
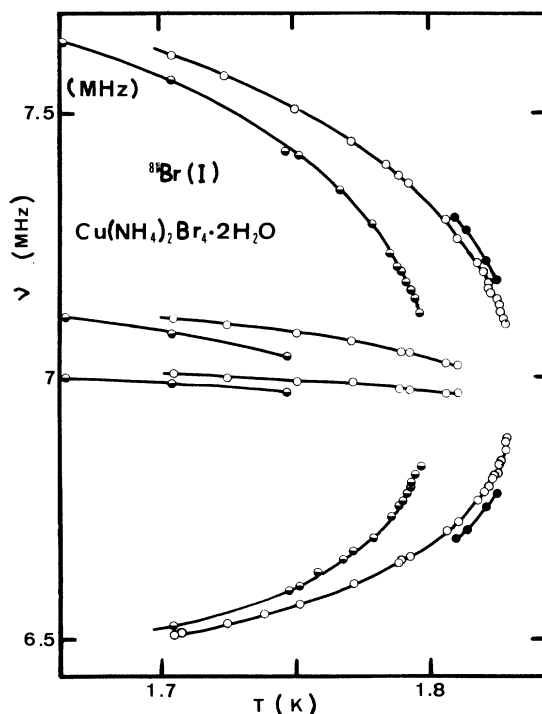
FIG. 8. Influence of the chlorine impurities in $Cu(NH_4)_2Br_4 \cdot 2H_2O$. Samples represented by ●, ○ and ◒ contain an increasing quantity of impurities.

E. VELU, J-P. RENARD, AND B. LECUYER

TABLE VI. Curie temperatures and experimental values of the parameters β and B.

		T_c (K)	β	B
$Cu(NH_4)B_2Br_4 \cdot 2H_2O$	A	$1.8346 \pm 3 \times 10^{-4}$	0.375 ± 0.008	1.45 ± 0.04
	B	$1.8306 \pm 3 \times 10^{-4}$	$10^{-3} < \|\epsilon\| < 7 \times 10^{-2}$	
$CuRb_2Br_4 \cdot 2H_2O$		$1.8762 \pm 2 \times 10^{-4}$	0.373 ± 0.007	1.45 ± 0.03
			$4 \times 10^{-4} < \|\epsilon\| < 7 \times 10^{-2}$	
$CuK_2Cl_4 \cdot 2H_2O$		$0.892 \pm 5 \times 10^{-4}$	0.354 ± 0.01	1.36 ± 0.06
			$2 \times 10^{-3} < \|\epsilon\| < 10^{-1}$	

metrical with respect to the mean frequency, with temperature-independent splittings. The complexity of this spectrum as well as the observed splittings between the lines can be explained if we take into account the dipolar interactions, not only between the protons of one water molecule, but also between the protons of two adjacent water molecules, separated by a distance of only 2.88 Å in $CuK_2Cl_4 \cdot 2H_2O$, and also between protons and halogens, bound to water by a hydrogen bond, whose length is 2.2 Å in $CuK_2Cl_4 \cdot 2H_2O$ and 1.7 Å in $Cu(NH_4)_2Br_4 \cdot 2H_2O$.

The mean frequency of the spectrum $\nu(T)$ is proportional to the local field at the protons and therefore proportional to the spontaneous magnetization $M_s(T)$. The reduced spontaneous magnetization is given by $m_s(T) = M_s(T)/M_s(0) = \nu(T)/\nu(0)$. The frequency at $T = 0$ K is extrapolated from the very low-temperature data obtained in an adiabatic demagnetization apparatus[25] (Table V). For the three salts, we note that the experimental curve $M_s(T)$ is located above the theoretical curve, as calculated by a spin-wave renormalization method

for the isotropic Heisenberg model with next-nearest-neighbor interactions.[3,22]

1. Bromine compounds [Fig. 10(a)]

In a previous paper[3] we have computed theoretical spontaneous magnetization curves for the Heisenberg model with a small anisotropy and with a next-nearest-neighbor interaction J_2 of the order of $\frac{1}{4}$ of the nearest-neighbor interaction J_1. We have generalized this computation to the case $J_2 = J_1$. The theoretical curves vary little as a function of the J_2/J_1 value. The experimental curve, identical for the two bromine compounds, is properly fitted by the theoretical curve for $J_1 = J_2$ and $H_A/T_c = 135$ Oe K^{-1} for $T/T_c < 0.5$. The corresponding H_A values which are given in Table V are consistent with those of Table IV.

2. $CuK_2Cl_4 \cdot 2H_2O$ [Fig. 10(b)]

The experimental curve is almost identical to that of the bromine compounds. It is not fitted by the theoretical curve for a planar anisotropy, computed by the spin-wave method without renormalization.[23] If the anisotropy were planar or almost planar, the magnetization of a domain would be badly fixed along the easy axis and it would fluctuate in the easy plane. Therefore the NMR lines, for instance, of chlorine would be much broader in the ferromagnetic state than in the paramagnetic state. In fact, though, we do not observe such a phenomenon. Furthermore the chlorine spectra clearly show that the spontaneous magnetization of a domain can only occur along the two directions [110] and [1$\bar{1}$0]. In a domain, everything happens as though one direction were favored with respect to the others and as though the anisotropy were either axial or rhombic. This is corroborated by the fact that the low-temperature spontaneous magnetization of a domain is the same as that of the bromine compounds, though theoretically the magnetization of a system with planar anisotropy noticeably differs from that of a system with uni-
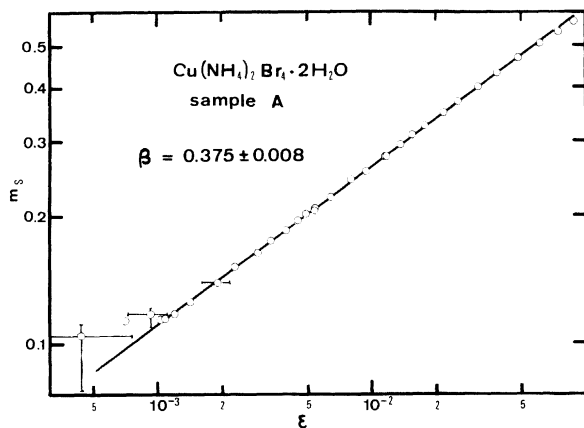

FIG. 9. $Cu(NH_4)_2Br_4 \cdot 2H_2O$. Temperature dependence of the reduced spontaneous magnetization near T_c plotted in a double logarithmic scale.
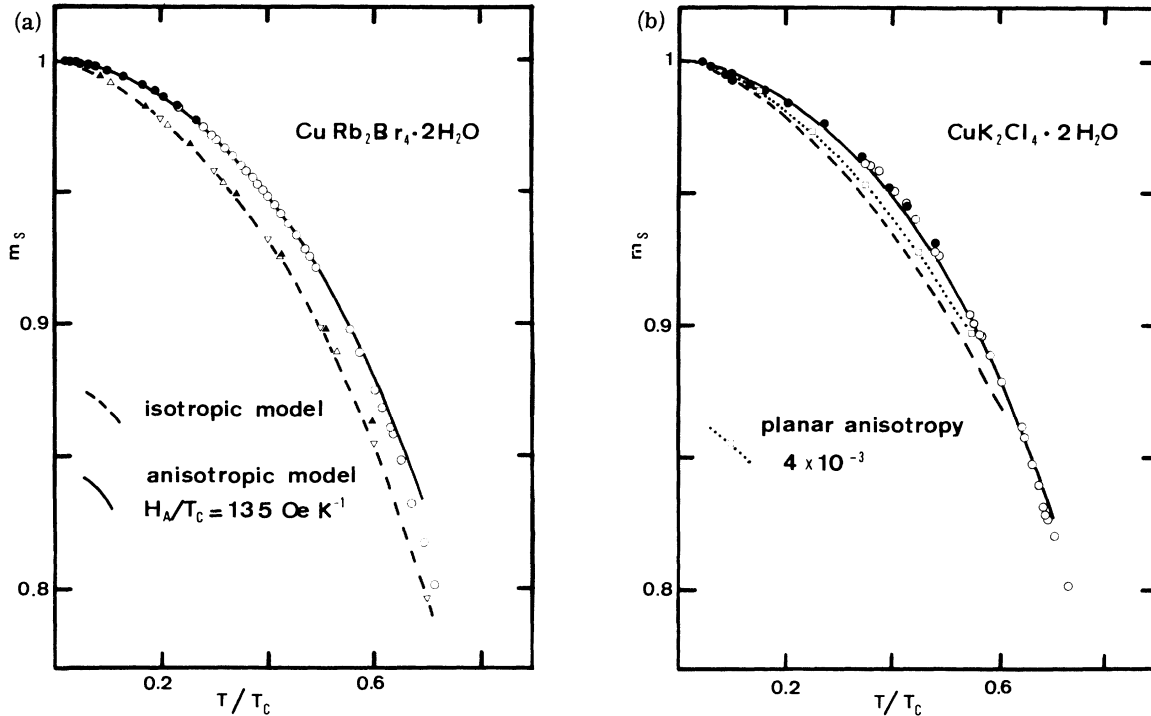
FIG. 10. Temperature dependence of the reduced spontaneous magnetization for $T < 0.6T_c$. $\bigcirc$: experiments in a ^{3}He bath; $\bullet$: experiments in an adiabatic demagnetization apparatus. (a) CuRb$_2$Br$_4$·2H$_2$O; (– – – –): theoretical curve for the isotropic model calculated with a spin-wave renormalization. $\triangle$: $J_2 = \bigcirc$; $\blacktriangle$: $J_2 = 0.25J_1$; ∇: $J_2 = J_1$. (———): theoretical curve calculated for a uniaxial anisotropy $H_A/T_c = 135$ OeK^{-1} with a spin-wave renormalization. (b) CuK$_2$Cl$_4$·2H$_2$O. (– – – –): theoretical curve for the isotropic model without renormalization; ($\cdots\square\cdots$): theoretical curve for a planar anisotropy equal to 4×10^{-3} without renormalization; (———): theoretical curve for a uniaxial anisotropy $H_A/T_c = 135$ OeK^{-1} with renormalization.

axial anisotropy. However, the tetragonal crystal symmetry prevents the singling out of one of the directions [110] or [1$\bar{1}$0]. We therefore assume that the crystal symmetry is modified at T_c by magnetostriction.[20] In support of this hypothesis is the significant variation below T_c of the parameters of the Cl(II) NMR, in the case where the spontaneous magnetization is parallel to [γ]. So the [110] axis becomes the favored axis for half of the domains and the [1$\bar{1}$0] axis the favored one for the other half. The macroscopic crystal symmetry of the susceptibility is not modified by the magnetostriction because just as many domains are magnetized along [110] as along [1$\bar{1}$0], and the two directions are macroscopically equivalent.

In a domain, the Hamiltonian of CuK$_2$Cl$_4$·2H$_2$O is therefore given by Eq. (7), where now z is the easy axis [110] or [1$\bar{1}$0], and where $\sum_{ij} K_{ij} > 0$.

VI. INDUCED MAGNETIZATION: CRITICAL ISOTHERM

The induced magnetization is measured by means of a fluxmetric method[24] (Fig. 11). The output sig-

nal of the integrator is proportional to the magnetization M of the sample. It is sent along the Y channel of a XY recorder.
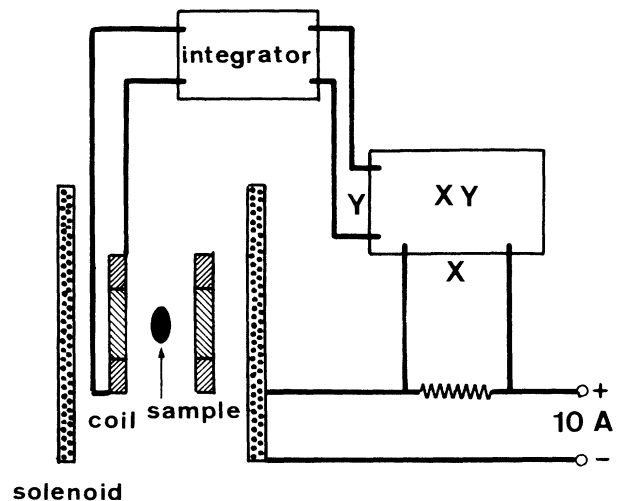

FIG. 11. Block diagram of the induced magnetization measurements apparatus.

The magnetic field H_0 is supplied by a solenoid whose homogeneity over the length of the flux-metric coil is better than 10^{-3}. A signal proportional to the current and therefore to H_0 is sent on the X channel of the recorder. One can increase the current proportionally with time.

The field variation speed is chosen to be sufficiently slow, in order to avoid any detectable heating of the sample. The variation times from 0- to 340 G range from 2 min in superfluid ^{4}He to 8 min in ^{3}He. We thus obtain the curve $M(H_0)$ directly on the recorder.

In order to calibrate the Y axis, we plot the curve $M(H_0)$ for a ferrite sphere at 4.2 K. The apparent volume susceptibility is independent of the field and is equal to $1/N$ and one should observe a straight line with a slope equal to $1/N$. The value of the experimental slope permits us to compute the calibration factor. Let H be the magnetic field inside the sample. To deduce the curves $M(H)$ from the curves $M(H_0)$, we use the equation

$$H = H_0 - NM. \tag{9}$$

The samples used are those which served for the susceptibility measurements. They are cut into ellipsoids and the demagnetizing factors N are known within an accuracy of 2% to 5%.

The magnetic field H_0 is applied along an easy axis. For the bromine compounds, the curves $M(H_0)$ are plotted at many temperatures, most of them in the range $-10^{-1} < \epsilon < 10^{-1}$. These curves allow us to determine the state equation (Sec. VII B). The critical isotherm is the curve $M(H)$ at $T = T_c$. For all the fields which we explored, it is well fitted by the law (Fig. 12)

$$m = M/M_0 = \Delta \cdot H^{1/\delta}. \tag{10}$$

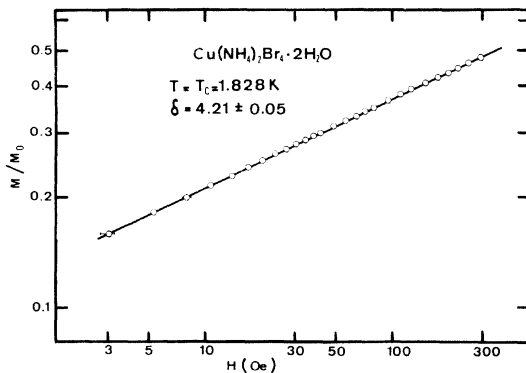The Δ and δ numerical values are given in Table VII. The uncertainty in δ arises especially from

FIG. 12. Critical isotherm of $Cu(NH_4)_2Br_4 \cdot 2H_2O$ plotted in a double logarithmic scale.

TABLE VII. Experimental values of the parameters δ and Δ of the critical isotherm.

	T_c (K)	δ	Δ
$Cu(NH_4)Br_4 \cdot 2H_2O$	1.828	4.21 ± 0.05 $3 < H < 300$ G	0.126 ± 0.003
$CuRb_2Br_4 \cdot 2H_2O$	1.874	4.20 ± 0.07 $2 < H < 300$ G	0.123 ± 0.003
$CuK_2Cl_4 \cdot 2H_2O$	0.895	4.4 ± 0.15 $1 < H < 100$ G	0.157 ± 0.01

the uncertainties in the demagnetizing factor and in T_c. Indeed, the curves $M(H_0)$ do not permit us to determine T_c accurately because they vary little near T_c. Since we have used the same samples in these experiments as those used in the $\chi_\parallel$ measurements, the chosen T_c is the critical temperature deduced by the Kouvel and Fisher method (Table III).

For $CuK_2Cl_4 \cdot 2H_2O$, the $M(H_0)$ measurements are less accurate. We have only plotted the curves $M(H_0)$ for T very close to T_c. The uncertainties in δ and Δ are greater than for the bromine compounds.

VII. DISCUSSION OF THE RESULTS IN THE NEIGHBORHOOD OF T_c

A. Scaling laws and the state equation

The experimental values of α, β, γ, and δ and the theoretical ones are given in Table VIII. As a rule the theoretical exponents computed from the high-temperature series expansions are more accurate than those computed by means of the $4 - d$ developments. We note that the experimental β exponent is consistent with the theoretical value of the Heisenberg model, but the latter is rather inaccurate. On the other hand, the experimental values of the other three exponents differ from the computed values. The experimental values of α and γ are intermediate between those of the Heisenberg model and those of the Ising model. As for δ, it is smaller than either of the two theoretical values. The scaling laws

$$2 - \alpha = 2\beta + \gamma = \beta(\delta + 1) = \gamma(\delta +)/(\delta - 1)$$

are checked in Table IX. They are not quite fulfilled by our salts: in particular, δ seems to be too small.

In accordance with the scaling hypothesis, the state equation must be of the form[25]

TABLE VIII. Experimental critical exponents $\beta, \gamma, \delta, \alpha$ compared with theoretical values for three-dimensional models.

	β	γ	δ	$\alpha = \alpha'$
$Cu(NH_4)_2Br_4 \cdot 2H_2O$	0.375 ± 0.008 $10^{-3} < \lvert \epsilon \rvert < 7 \times 10^{-2}$	1.275 ± 0.017 $2 \times 10^{-3} < \epsilon < 2.2 \times 10^{-1}$	4.21 ± 0.05 $3 < H < 300$ G	
$CuRb_2Br_4 \cdot 2H_2O$	0.373 ± 0.007 $4 \times 10^{-4} < \lvert \epsilon \rvert < 7 \times 10^{-2}$	1.29 ± 0.01 $5 \times 10^{-3} < \epsilon < 3 \times 10^{-1}$	4.20 ± 0.07 $2 < H < 300$ G	-0.041 ± 0.014 [a]
$CuK_2Cl_4 \cdot 2H_2O$	0.354 ± 0.010 $2 \times 10^{-3} < \lvert \epsilon \rvert < 10^{-1}$	1.28 ± 0.01 $1.5 \times 10^{-3} < \epsilon < 3 \times 10^{-1}$	4.4 ± 0.15 $1 < H < 100$ G	
High-temperature expansion				
Heisenberg	0.35 ± 0.05	$1.375^{+0.02}_{-0.01}$	5.0 ± 0.2	-0.14 ± 0.06
Ising	0.313 ± 0.003	1.25	5.0 ± 0.2	0.13 ± 0.01
$4-d$ expansion				
Heisenberg	0.380	1.365	4.458	-0.125
Isotropic dipolar	0.381	1.372	4.454	-0.135
Molecular field	0.5	1	3	Discontinuity

[a] Reference 7.

$$m/H^{1/\delta} = g(\epsilon/H^{1/\beta\delta})$$

or[26]   (11)

$$H/m^\delta = h(\epsilon/m^{1/\beta}).$$

From the universality hypothesis, the functions h and g do not depend upon either spin or lattice, but do depend upon the number of spin components, upon the lattice dimensionality, and perhaps upon other factors such as the anisotropy. The state equation of the bromine compounds is obtained from the induced magnetization curves plotted at many temperatures.[27] In Fig. 13, we compare the experimental curve of $Cu(NH_4)_2Br_4 \cdot 2H_2O$ with the theoretical curves for the $S = \frac{1}{2}$ Heisenberg and Ising models computed for the bcc lattice.[28] The abscissa and ordinate are dimensionless $(1/\Delta M_0)$ $\times (M/H^{1/\delta})$ in the ordinate and $(B/\Delta)^{1/\beta}(\epsilon/H^{1/\beta\delta})$ in the abscissa.

We are not able to calculate simply the uncertainty in the abscissa and ordinate due to those in β, δ, B, and Δ. We should observe that the differences between β and B and their mean values are correlated as well as those of δ and Δ. A calculation done with a few points and using the ex-

tremal values of β and δ shows that the curve depends very little upon the β and δ values when the abscissa lies between 2 and -2. The uncertainty increases as the abscissa increases. Finally, the experimental curve is well fitted by the theoretical state equation of the Heisenberg model and it is clearly distinct from that of the Ising model.

B. Crossover

If the Heisenberg model accounts for the form of the state equation, it does not account for the critical exponents values and particularly not for the γ exponent, which is known with great accuracy. This phenomenon can only be attributed to the presence of the anisotropy[28] or of dipolar interactions between spins.[7]

Fisher and Aharony[6] have shown that dipolar interaction is a relevant operator. It follows if one neglects the anisotropy, that the system must gradually crossover from the Heisenberg model $\lvert \epsilon \rvert \gg \epsilon^*$ to the isotropic dipolar model $\lvert \epsilon \rvert \ll \epsilon^*$. The reduced crossover temperature ϵ^* is given by

TABLE IX. Experimental check of the scaling laws: $2 - \alpha = 2 - \alpha' = 2\beta + \gamma = \beta(\delta + 1) = \gamma(\delta + 1)/(\delta - 1)$.

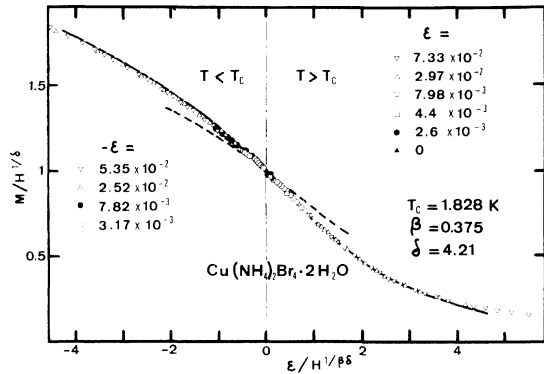|	$2 - \alpha = 2 - \alpha'$	$2\beta + \gamma$	$\beta(\delta + 1)$	$\gamma(\delta + 1)/(\delta - 1)$
$Cu(NH_4)_2Br_4 \cdot 2H_2O$		2.025 ± 0.033	1.954 ± 0.061	2.069 ± 0.040
$CuRb_2Br_4 \cdot 2H_2O$	2.041 ± 0.014	2.036 ± 0.024	1.940 ± 0.063	2.096 ± 0.033
$CuK_2Cl_4 \cdot 2H_2O$		1.988 ± 0.030	1.91 ± 0.11	2.032 ± 0.052

FIG. 13. Scaled state equation of $Cu(NH_4)_2Br_4 \cdot 2H_2O$ compared to the theoretical scaling function of the $S = \frac{1}{2}$ bcc Heisenberg (solid curve) and Ising (dotted curve) models.

$$\epsilon^* \sim [3\pi(g\mu_B)^2/zJv]^{1/\phi_D},$$

where g is the Landé factor, z is the number of equivalent neighbors, v is the unit-cell volume, and ϕ_D is the crossover exponent equal to

γ(Heisenberg) = 1.38. In our samples ϵ^* is of the order of 3×10^{-2} for bromine compounds and 6×10^{-2} for $CuK_2Cl_4 \cdot 2H_2O$, and this crossover occurs in the experimental range. The critical exponents should be intermediate between those of the Heisenberg model and those of the isotropic dipolar model. The latter were calculated by Bruce and Aharony[29]: they differ very little from those of the Heisenberg model (Table VIII). It is therefore not possible to explain the measured values of the critical exponents by taking only dipolar interactions into account.

Let us now consider the exchange anisotropy which also is a relevant parameter. Theoretically in the presence of a uniaxial exchange anisotropy, if one neglects the dipolar interaction, the system passes gradually from the Heisenberg model $|\epsilon| \gg \epsilon^*$ to the Ising model[4] $|\epsilon| \ll \epsilon^*$, where

$$\epsilon^* \sim \hat{g}^{1/\phi_A}.$$

ϕ_A is the exponent of the crossover due to the anisotropy, equal to 1.25.[5] $\hat{g}$ is a parameter proportional to the anisotropy: $\hat{g} = 4 \times 10^{-3}$ and ϵ^*
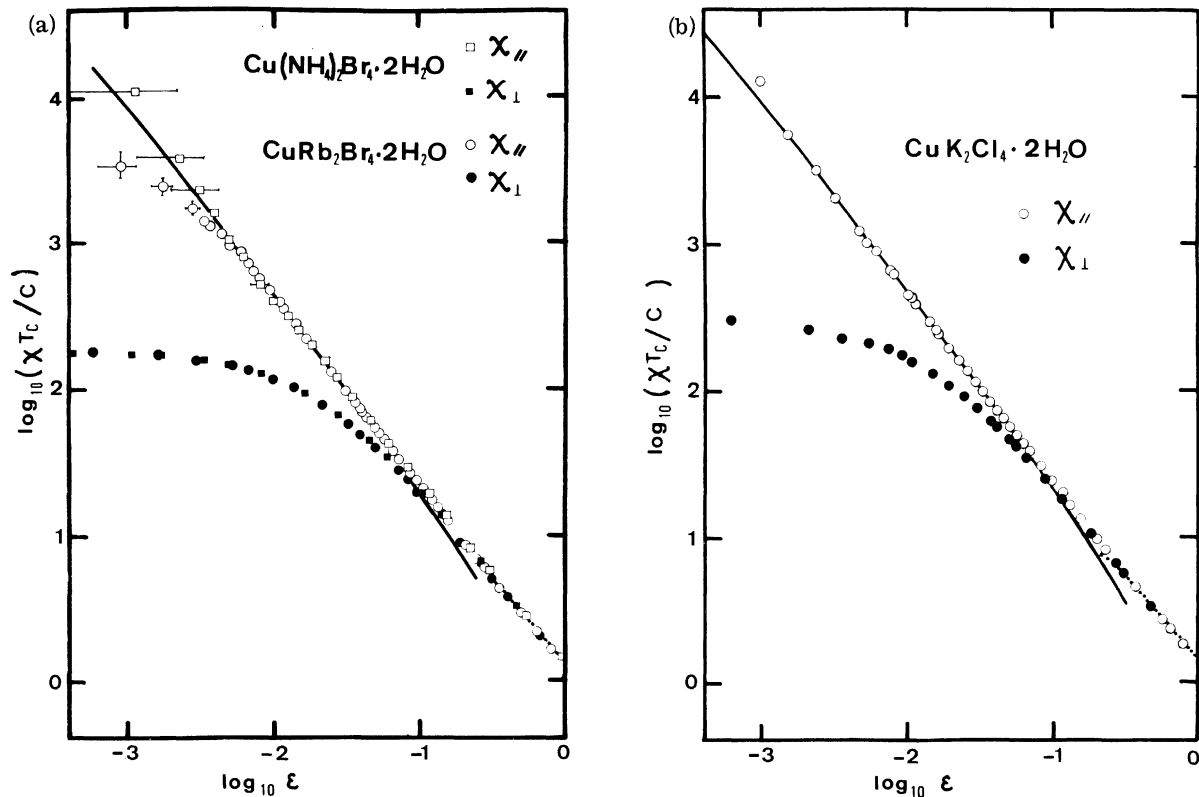

FIG. 14. Parallel and perpendicular susceptibilities vs temperature in a double logarithmic scale. Amplitude of the theoretical parallel susceptibility (solid curve) has been adjusted to fit the experimental data at $\epsilon = 10^{-2}$. For $\epsilon > 0.4$, the measured susceptibilities fit the dotted curve deduced from the high-temperature expansion for the $S = \frac{1}{2}$ bcc Heisenberg model. (a) Bromine compounds. Theoretical curve is calculated for $\hat{g} = 4 \times 10^{-3}$. (b) $K_2CuCl_4 \cdot 2H_2O$. Theoretical curve is calculated for $\hat{g} = 2 \times 10^{-3}$.

$= 1.2 \times 10^{-2}$ for the bromine compounds; $\hat{g} = 2 \times 10^{-3}$ and $\epsilon^* = 6.6 \times 10^{-3}$ for $CuK_2Cl_4 \cdot 2H_2O$.

This crossover is easily observable in the perpendicular susceptibility behavior $\chi_\perp$ (Fig. 14). For $\epsilon \gg \epsilon^*$, the system is isotropic and $\chi_\perp = \chi_\parallel$. On the other hand, for $\epsilon \ll \epsilon^*$, the system behaves like an Ising model and $\chi_\perp$ does not vary with the temperature. ϵ^* is roughly the reduced temperature at which the plot of $\log_{10}\chi_\perp$ vs $\log_{10}\epsilon$ has maximal curvature: 2×10^{-2} for the bromine compounds, 10^{-2} for $CuK_2Cl_4 \cdot 2H_2O$, which agrees with the computed crossover temperatures.

The perpendicular susceptibility maximum $\chi_\perp$ ($\epsilon = 0$) is theoretically proportional to $\hat{g}^{-\gamma/\phi} = \hat{g}^{-1.1}$. We indeed note that $\chi_\perp$ ($\epsilon = 0$) is greater for $CuK_2Cl_4 \cdot 2H_2O$ than for the bromine compounds. The ratio between the two maxima is consistent with the ratio of the $\hat{g}$ values, when one takes into account the incertainty in $\hat{g}$, which is of the order of 10%.

In Fig. 14, we have also compared the parallel susceptibility with the theoretical scaling function of the Heisenberg model with a small uniaxial exchange anisotropy.[5] Let $T_c(\hat{g})$ be the critical temperature of the anisotropic system and $T_c(0)$ that of the isotropic system. We put

$$t = T/T_c(0) - 1. \tag{12}$$

In the critical zone, the temperature dependence of $\chi_\parallel$ is given by

$$\chi_\parallel T/C = At^{-\gamma} X_\parallel(\hat{B}\hat{g}/t^{\phi_A}). \tag{13}$$

C is the Curie constant and γ is the Heisenberg exponent $= 1.38$. $X_\parallel$ is a universal function whose form is given by Eq. (7.11) and (7.15) of Ref. 5. A and $\hat{B}$ are nonuniversal constants depending upon the spin and the lattice. For a bcc lattice with only nearest-neighbor interactions, we have[30]

$$A = 1.177 \quad \text{for} \quad S = \tfrac{1}{2}$$

and[5]   (14)

$$\hat{B} = 1.183 \quad \text{for} \quad S = \infty.$$

The $\hat{B}$ value for a spin $S = \tfrac{1}{2}$ is not exactly known but in any case it is close to one.

The t variable is converted into the ϵ variable by means of the relation

$$T_c(\hat{g})/T_c(0) = 1 + (\hat{B}\hat{g}/1.29)^{1/\phi_A}. \tag{15}$$

Equation (13) is only valid in the critical zone, that is to say for $\epsilon < 10^{-1}$. The computation shows that the theoretical curve is insensitive to the $\hat{g}$ value: the curves computed for $\hat{g} = 4 \times 10^{-3}$ and $\hat{g} = 2 \times 10^{-3}$ are not perceptibly different. This allows us to make the theoretical computations with the $\hat{B}$ value given above although it does not cor-

respond to the experimental case. We have adjusted the A coefficient in such a way that the experimental curve coincides with the theoretical one at $\epsilon = 10^{-2}$.

For the three salts the ratio of the experimental A with the theoretical A given above is approximately 0.88. We attribute this lowering of the amplitude to the influence of the next-nearest-neighbor interactions, an effect which one can see on the high-temperature series expansions (Fig. 3).

The slope of the theoretical curve evolves very slowly from the Heisenberg γ to the Ising γ (three decades in ϵ). The local slope near $\epsilon = 10^{-2}$ is equal to 1.305 for the two $\hat{g}$ values. It is very close to the experimental value of the γ exponent. In fact, in the interval $10^{-3} < \epsilon < 10^{-1}$, we measure an effective critical exponent intermediate between the Heisenberg and Ising ones.

The Heisenberg behavior of the susceptibility is hidden by the fact that the system behavior progressively becomes "classical" for $\epsilon > 10^{-1}$; it goes out of the critical zone. So we observe a kind of crossover between critical behavior and molecular-field behavior. The reduced temperature of this "crossover" is given by the Ginzburg criterion: the greater the interactions range, the lower this reduced temperature; in our case, it is of the order of 5×10^{-1}. Thus, above $\epsilon = 3 \times 10^{-1}$, the experimental data are much better fitted by the high-temperature series expansion than by Eq. (13).

C. Conclusion

In the immediate vicinity of T_c, since the system exhibits an Ising-like behavior, the effect of the dipolar interactions must be reconsidered. Several authors[31] have shown that dipolar interactions in a uniaxial Ising-like system strongly affect the critical behavior and give the exponent values of the Landau model. In the present work, we believe that we observe both previously discussed crossovers: a first crossover due to the anisotropy which lowers the symmetry of short-range interactions and a second crossover due to the dipolar interactions in the resulting Ising-like system. The two-crossover hypothesis might explain the experimental values of the critical exponents which are all shifted towards the values of the molecular-field model.

Lastly, because our experiments have been done in the crossover region, the measured exponents are effective exponents: hence it is not surprising that they do not exactly satisfy the scaling laws. For these nonideal ferromagnets the scaling laws are only valid in the immediate neighborhood of T_c: $\epsilon < 10^{-4}$.

APPENDIX A: FIELD DEPENDENCE OF $\chi_\perp$ AT $T = 0K$

We perform here a molecular-field treatment. The results are exact at $T = 0$ K and are approximate for $T \ll T_c$. When there is no magnetic field, the Hamiltonian is

$$\mathcal{H}_0 = -\sum_{ij} J_{ij}\vec{S}_i \cdot \vec{S}_j - \sum_{ij} K_{ij} S_{iz}S_{jz}.$$ (A1)

The sums $\sum_{ij}$ are extended to the nearest and next-nearest neighbors i and j. Later on, the $\vec{S}$ operators are taken as classical vectors. We limit the study to the case of the uniaxial anisotropy ($\sum_{ij} K_{ij} > 0$). The planar anisotropy is treated in the same manner, but

$$+ \sum_{ij} K_{ij} S_{ix} S_{jx}$$

is substituted for

$$- \sum_{ij} K_{ij} S_{iz}S_{jz}.$$

The z axis is an easy axis; the x axis is a hard axis.

We neglect the dipolar interactions. We define the "anisotropy field" H_A by[3] (Appendix B):

$$ng_z\mu_B H_A = 2S\sum_{ij} K_{ij},$$ (A2)

where n is the number of spins and g_z is the J andé factor in the z direction.

The sample is an ellipsoid with axes x, y, and z and respective demagnetizing factors N_x, N_y, and N_z. At $T = 0$ K, all spins are parallel to the z-direction axis. We apply an external magnetic field to the system.

1. Magnetic field H_x is parallel to the x direction

The spins turn in the xz plane and a magnetization parallel to the x axis appears:

$$M_x = ng_x\mu_B S \sin\theta,$$
$$S_z = S\cos\theta.$$ (A3)

θ is the angle of the spins with the z axis. The energy of the system is

$$E = -\sum_{ij} J_{ij}\vec{S}_i \cdot \vec{S}_j - \sum_{ij} K_{ij} S_{iz}S_{jz}$$
$$- M_x H_x + \tfrac{1}{2}N_x M_x^2$$ (A4)

The last term represents the potential energy due to the demagnetizing field.
Combining Eqs. (A3) and (A4) we get

$$E' = \frac{E}{ng_x\mu_B S} = E_0' + \frac{1}{2}\left(H_A\frac{g_z}{g_x} + D_x\right)\sin^2\theta - H_x\sin\theta.$$ (A5)

E_0' is a constant and D_x is the maximal intensity of the demagnetizing field in the x direction: $D_x = N_x ng_x\mu_B S$. We look for the θ values which minimize E'.

(a) $H_x < H_A g_z/g_x + D_x$. The solution is given by

$$\sin\theta = \frac{H_x}{H_A g_z/g_x + D_x}.$$

The apparent perpendicular susceptibility is constant:

$$\chi_{ax} = \frac{ng_x\mu_B S}{H_A g_z/g_x + D_x}.$$ (A6)

(b) $H_x > H_A g_z/g_x + D_x$. We have $\sin\theta = 1$, $\cos\theta = 0$, and

$$\chi_{ax} = 0.$$ (A7)

The curve of the apparent perpendicular susceptibility versus H_x has the form of a step whose height and length permit us to calculate H_A [Fig. 15(a)].

2. Magnetic field H_z is parallel to the z direction

We add a small field h, parallel to the x direction, to measure the perpendicular susceptibility. We note that $D_z = N_z ng_z\mu_B S$. The method is identical to the one in the previous paragraph.

$$E' = E_0' + \tfrac{1}{2}(H_A g_z/g_x + D_x)\sin^2\theta$$
$$- h\sin\theta - M_z H_z + \tfrac{1}{2}N_z M_z^2$$ (A8)

(a) $H_z < D_z$. M_z adjusts itself so that the demagnetizing field cancels the applied field in the sample:

$$M_z = H_z/N_z,$$

$$E' = E_0' - \frac{H_z^2}{2N_z} + \frac{1}{2}\left(H_A\frac{g_z}{g_x} + D_x\right)\sin^2\theta - h\sin\theta.$$ (A9)

This equation only differs from Eq. (A5) by a constant. Whence
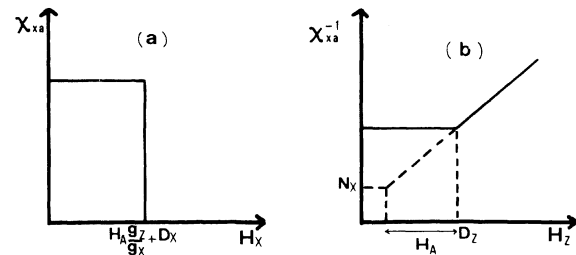

FIG. 15. Theoretical variation of the apparent perpendicular susceptibility as a function of an applied field $\vec{H}$. (a) $\vec{H}$ is parallel to the direction along which the susceptibility is measured. (b) $\vec{H}$ is parallel to an easy axis.

$$\frac{1}{\chi_{ax}} = \frac{1}{ng_x\mu_B S}H_A\frac{g_z}{g_x} + N_x. \tag{A10}$$

(b) $H_z > D_z$; the Bloch walls no longer exist

$$M_z = ng_z\mu_B S\cos\theta.$$

E' is expressed in the parameter θ and minimized. We obtain

$$\frac{1}{\chi_{ax}} = \frac{1}{ng_x\mu_B S}\left(\frac{g_z}{g_x}(H_z - D_z + H_A) + N_x\right). \tag{A11}$$

Thus the curve $1/\chi_{ax}$ vs H_z gives us another evaluation of H_A [Fig. 15(b)].

APPENDIX B: INFLUENCE OF THE UNIAXIAL ANISOTROPY ON THE PERPENDICULAR SUSCEPTIBILITY FOR $T < 0.5\,T_c$

This calculation used the results obtained in a previous paper,[3] where we calculated the renormalized-spin-wave spectrum in the case of the Heisenberg Hamiltonian with a small uniaxial anisotropy and with next-nearest-neighbor interactions.

The Hamiltonian is

$$\mathcal{K} = \mathcal{K}_0 + V,$$

where

$$\mathcal{K}_0 = -\sum_{ij}J_{ij}\vec{S}_i\cdot\vec{S}_j - \sum_{ij}K_{ij}S_{iz}S_{jz}, \tag{B1}$$

$$V = -g_x\mu_B h\sum_i S_{ix}.$$

V represents the potential due to the small field h parallel to the x axis which one needs to measure the perpendicular susceptibility. h is sufficiently small for V to be a perturbation with respect to $\mathcal{K}_0$.

We generalize the previous results[3] in the case where $K_{ij} \neq 0$ for the couples i and j nearest and next-neighbors and where

$$0 < \sum_{ij}K_{ij} \ll \sum_{ij}J_{ij}.$$

We write $\mathcal{K}_0$ in the form

$$\mathcal{K}_0 = E_0 + \sum_k \bar{\omega}_k a_k^\dagger a_k, \tag{B2}$$

where $a_k^\dagger$ and a_k are the creation and annihilation operators of a spin wave vector $\vec{k}$, $\bar{\omega}_k$ is the renormalized energy of this spin wave, and E_0 is a constant.

$$\bar{\omega}_k = \alpha_1(T)\epsilon_k^1 + \alpha_2(T)\epsilon_k^2 + 2S\sum_i K_i\gamma_i(0)\beta_i(\vec{k},T); \tag{B3}$$

$$\alpha_i(T) = 1 - \frac{1}{2nS^2 J_i\gamma_i(0)}\sum_{k'}n_{k'}\epsilon_{k'}^i,$$

$$\beta_i(\vec{k},T) = 1 - \frac{1}{nS}\sum_{k'}\left(1 + \frac{\gamma_i(\vec{k})\gamma_i(\vec{k}')}{\gamma_i^2(0)}\right)n_{k'}. \tag{B4}$$

n is the number of spins. The other notations are the same as those of Ref. 3.

The anisotropy field H_A is defined by

$$g_z\mu_B H_A = 2S\sum_i K_i\gamma_i(0). \tag{B5}$$

We call $|p_0, \ldots, p_k, \ldots\rangle$ the eigenvector of $\mathcal{K}_0$ which represents the state where there exists p_0 spin waves of wave vector 0 and p_k spin waves of wave vector $\vec{k}$. $p_0, \ldots, p_k$ are positive or null integers. $\mathcal{K}_0$ is diagonal in the basis composed by all the $|p_0, \ldots, p_k, \ldots\rangle$. In the statistical equilibrium at temperature T, we have

$$n_k = \langle a_k^\dagger a_k\rangle = \langle p_k\rangle = (e^{\bar{\omega}_k/k_B T} - 1)^{-1}. \tag{B6}$$

When one successively applies Holstein-Primakoff and Fourier transforms, one gets an expression of the perturbation V as a function of the $a_k^\dagger$ and a_k operators up to third order

$$V = -g_x\mu_B h\frac{(2nS)^{1/2}}{2}\left((a_0 + a_0^\dagger) - \frac{1}{4nS}\sum_{kk'}a_k^\dagger a_{k'}^\dagger a_{k+k'}\right.$$

$$\left. - \frac{1}{4nS}\sum_{kk'}a_{k+k'}^\dagger a_k a_{k'}\right). \tag{B7}$$

We make the following assumptions: (i) We treat the perturbation in the nondegenerate case. These assumptions were already done in the renormalization calculation. We see that V does not contain diagonal terms and we must drive the calculation up to the second order of the perturbation. (ii) The three-operator terms are small with respect to the one-operator terms. We only keep those which contain $a_k^\dagger a_k$, that is to say the terms which modify only one quantum number p and which concern only one spin wave. These terms verify:

$$\vec{k} + \vec{k}' = \vec{k}, \quad \text{or} \quad \vec{k} + \vec{k}' = \vec{k}';$$

that is to say $\vec{k} = 0$ or $\vec{k}' = 0$. Hence V becomes

$$V = g_x\mu_B h\frac{(2Sn)^{1/2}}{2}(a_0 + a_0^\dagger)\left(1 - \frac{1}{2nS}\sum_k a_k^\dagger a_k\right). \tag{B8}$$

The calculation of the perpendicular susceptibility is of the following: (1) we calculate the perturbed basis states up to the first order in V: $|p_0', p_k'\rangle$. (2) We calculate the mean value of $\sum_i S_{ix}$ in the new basis states:

$$\left\langle p_0', p_k'\left|\sum_i S_{ix}\right|p_0', p_k'\right\rangle.$$

(3) Lastly we calculate the statistical mean value of $\sum_i S_{ix}$ denoted as $\langle \sum_i S_i \rangle$, summing on all states, taking into account their probability. The magne-

tization along x axis is proportional to $\langle \sum_i S_{ix} \rangle$.

Let $\lambda = g_x \mu_B h (2Sn)^{1/2}/2$. The perturbed eigen-vector is written up to the first order in λ:

$$|p_0', p_k'\rangle = |p_0, p_k\rangle + \lambda \left(1 - \frac{1}{2nS} \sum_k p_k\right) \left(\frac{(p_0)^{1/2}}{\tilde{\omega}_0} |p_0 - 1, p_k\rangle - \frac{(p_0 + 1)^{1/2}}{\tilde{\omega}_0} |p_0 + 1, p_k\rangle\right).$$ (B9)

Using Eqs. (B8) and (B9), we obtain Eq. (B10).

$$\sum_i S_{ix} |p_0', p_k'\rangle = \frac{(2Sn)^{1/2}}{2} \left[\left(1 - \frac{1}{2nS} \sum_k p_k\right)[\sqrt{p_0}|p_0 - 1, p_k\rangle + (p_0 + 1)^{1/2} |p_0 + 1, p_k\rangle] - \frac{\lambda}{\tilde{\omega}_0}\left(1 - \frac{1}{2nS} \sum_k p_k\right)^2 |p_0, p_k\rangle\right.$$

$$\left. + (\text{terms in } |p_0 + 2, p_k\rangle \text{ and } |p_0 - 2, p_k\rangle)\right].$$ (B10)

We have neglected $1/2nS$ with respect to 1. In the end, the mean value of $\sum_i S_{ix}$ in the $|p_0', p_k'\rangle$ state is:

$$\langle p_0', p_k' | \sum_i S_{ix} |p_0', p_k'\rangle = -\frac{\lambda}{\tilde{\omega}_0}\left(1 - \frac{1}{2nS} \sum_k p_k\right)^2 (2Sn)^{1/2}.$$ (B11)

Probability of finding the system in the $|p_0, p_k\rangle$. This is proportional to

$$\exp\left(-\frac{1}{k_B T} \sum_k \tilde{\omega}_k p_k\right).$$

At low temperature, the most probable states are those with small p_k such that $(1/2nS)\sum_k p_k \ll 1$.

So we can write

$$\langle p_0', p_k' | \sum_i S_{ix} |p_0', p_k'\rangle = -\frac{\lambda}{\tilde{\omega}_0}\left(1 - \frac{1}{nS} \sum_k p_k\right)(2Sn)^{1/2}$$

and

$$\langle \sum_i S_{ix} \rangle = -\frac{\lambda}{\tilde{\omega}_0}(2Sn)^{1/2}\left(1 - \frac{1}{nS} \sum_k \langle p_k \rangle\right)$$

$$= -\frac{\lambda}{\tilde{\omega}_0}(2Sn)^{1/2}\left(1 - \frac{1}{nS} \sum_k n_k\right)$$

$$= -\frac{\lambda}{\tilde{\omega}_0}(2Sn)^{1/2} m(T).$$ (B12)

The magnetization parallel to the x axis is

$$M_x = g_x \mu_B \left\langle \sum_i S_{ix} \right\rangle = g_x^2 \mu_B^2 Sn \frac{m}{\tilde{\omega}_0} h.$$ (B13)

Following Eqs. (B3) and (B4), we have

$$\tilde{\omega}_0 = 2S \sum_i K_i \gamma_i(0) \beta_i(0, T)$$

$$= 2S \sum_i K_i \gamma_i(0)[2m(T) - \alpha_i(T)].$$ (B14)

Noting that for $T < 0.5T_c$, α_1 is very close to α_2,[3,32] and we obtain, using Eq. (B5):

$$\tilde{\omega}_0 = 2S[2m(T) - \alpha_1(T)] \sum_i K_i \gamma_i(0)$$

$$= g_z \mu_B H_A [2m(T) - \alpha_1(T)].$$ (B15)

From Eqs. (B13) and (B15) we deduce the per-pendicular susceptibility

$$\chi_x(T) = \frac{M_x}{h} = n \frac{g_x^2}{g_z} \mu_B S \frac{1}{H_A} \frac{m(T)}{2m(T) - \alpha_1(T)}.$$ (B16)

At $T = 0$ K, $m = 1$ and $\alpha_1 = 1$, and we find again Eq. (6), which had previously been deduced from molecular field theory.

The $m/(2m - \alpha_1)$ factor gives the temperature dependence of χ_x. This is plotted in Fig. 16 in re-duced scale. As for all spin-wave calculations, this one is only valid if there are few spin waves, that is to say for $T < 0.5T_c$.
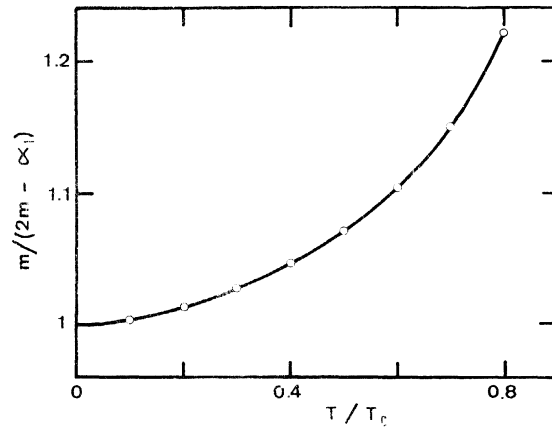

FIG. 16. Theoretical temperature dependence of the perpendicular susceptibility for $T < 0.6T_c$ on a reduced scale.

†This work is part of the Ph.D. thesis of Elisabeth Velu, CNRS Report No. A.O.11243 (unpublished).

[1]D. W. Wood and N. W. Dalton, Proc. Phys. Soc. Lond. 87, 755 (1966).

[2]W. D. Van Amstel and L. J. de Jongh, Solid State Commun. 14, 491 (1974).

[3]E. Vélu, J. P. Renard, and C. Dupas, Solid State Commun. 11, 1 (1972).

[4]E. Riedel and F. Wegner, Z. Phys. 225, 195 (1969).

[5]P. Pfeuty, D. Jasnow, and M. E. Fisher, Phys. Rev. B 10, 2088 (1974).

[6]M. E. Fisher and A. Aharony, Phys. Rev. Lett. 30, 559 (1973); Phys. Rev. B 8, 3323 (1973).

[7]F. L. Lederman, M. B. Salamon, and L. W. Shacklette, Phys. Rev. B 9, 2981 (1974).

[8]R. W. G. Wyckoff, Crystal Structures, 2nd ed. (Interscience, New York, 1965); Vol. 3, p. 617; R. Chidambaram, et al., Acta Crystallogr. B 26, 827 (1970).

[9]J. R. Clément and E. H. Quinnel, Phys. Rev. 79, 1028 (1950); Rev. Sci. Instrum. 23, 213 (1952).

[10]B. Lécuyer, Thèse d'Ingénieur (Conservatoire National des Arts et Métiers, Paris, 1969) (unpublished).

[11]A. R. Miedema, H. Van Kempen, and W. J. Huiskamp, Physica (Utr.) 29, 1266 (1963).

[12]E. Vélu and J. P. Renard, C. R. Acad. Sci. B 280, 657 (1975).

[13]N. W. Dalton and D. W. Wood, Phys. Rev. 138, A779 (1965).

[14]D. W. Wood and N. W. Dalton, Phys. Rev. 159, 384 (1967).

[15]G. A. Baker, H. E. Gilbert, J. Eve, and G. S. Rushbrooke, Phys. Rev. 164, 800 (1967).

[16]J. S. Kouvel and M. E. Fisher, Phys. Rev. 136, A1626 (1964).

[17]H. Suzuki and T. Watanabe, J. Phys. Soc. Jpn. 30, 367 (1971).

[18]L. J. De Jongh and A. R. Miedema, Physica (Utr.) 46, 44 (1970).

[19]H. Suzuki and T. Watanabe, Phys. Lett. A 26, 103 (1967).

[20]T. O. Klaassen, Thesis (Leiden, 1973) (unpublished); T. O. Klaassen, A. Gevers, and N. J. Poulis, Physica (Utr.) 61, 95 (1972); T. O. Klaassen, A. Gevers, W. J. Lovyestijn, and N. J. Poulis, ibid. 64, 149 (1973).

[21]J. P. Renard and E. Vélu, J. Phys. (Paris) C 1, 1154 (1971).

[22]C. Dupas, J. P. Renard, and E. Vélu, J. Low Temp. Phys. 2, 355 (1972); P. Beauvillain (private communication).

[23]T. Oguchi, J. Phys. Soc. Jpn. 30, 988 (1971).

[24]E. Vélu, D. Cadoul, B. Lécuyer, and J. P. Renard, Phys. Lett. A 36, 443 (1971).

[25]R. B. Griffiths, Phys. Rev. 158, 176 (1967).

[26]S. Milosevic and H. E. Stanley, Phys. Rev. B 6, 986 (1972); 1002 (1972).

[27]E. Vélu, B. Lécuyer, and J. P. Renard, Solid State Commun. 17, 515 (1975).

[28]L. J. De Jongh and A. R. Miedema, Adv. Phys. 23, 1 (1974).

[29]A. D. Bruce and A. Aharony, Phys. Rev. B 10, 2078 (1974).

[30]S. D. Ritchie and M. E. Fisher, Phys. Rev. B 5, 2668 (1972).

[31]A. I. Larkin and D. E. Khmel'instkii, Zh. Eksp. Teor. Fiz. 56, 2087 (1969) [Sov. Phys.-JETP 29, 1123 (1969)]; A. Aharony, Phys. Rev. B 8, 3363 (1973).

[32]P. D. Loly, J. Appl. Phys. 39, 1109 (1968).